Research Article

Abdulaziz Alangari, Mourad A. M. Aboul-Soud, Mohammed S. Alqahtani, Mudassar Shahid, Rabbani Syed, R. Lakshmipathy*, Jeevan Kumar Reddy Modigunta, Harshita Jaiswal, and Meenakshi Verma

Green synthesis of copper oxide nanoparticles using genus *Inula* and evaluation of biological therapeutics and environmental applications

https://doi.org/10.1515/ntrev-2024-0039
received December 17, 2023; accepted May 15, 2024

Abstract: In this research, we produced copper oxide nanoparticles (CuO NPs) using extracts from the entire aboveground portion of plants of genus Inula (*Inula graveolens*). The synthesis of CuO NPs was verified through various physicochemical analytical methods, including UV–visible, Fourier transform infrared, and transmission electron microscopy. The CuO NPs were found to be around 20 nm in size and spherical in shape. Subsequently, the synthesized compounds were evaluated for their anticancer properties. After treating A549 cells with CuO NPs at concentrations of 15 and 30 µg, we examined their cytotoxicity, lipid peroxidation activity (malondialdehyde level), and antioxidant activity (catalase, superoxide dismutase, and glutathione levels). Additionally, we analyzed the expression of apoptotic marker genes (p53, caspase-3, and caspase-9), cytokine levels (IL-6 and TNF-α), and DNA fragmentation. Our findings demonstrated that CuO NPs enhanced the expression of apoptotic genes, suggesting that phytochemical-derived NPs from Inula extracts induce apoptosis by upregulating tumor suppressor genes and downregulating oncogenes in A549 cells. Furthermore, CuO NPs exhibited higher susceptibility toward *B. subtilis* and *S. aureus* compared to ampicillin. Using the response surface methodology, we determined that CuO NPs are effective adsorbents for removing Pb^{2+} ions from aqueous solutions, making them promising for environmental applications. Overall, our results indicate that CuO NPs have potential as antimicrobial, antioxidant, and anticancer agents and as efficient adsorbents.

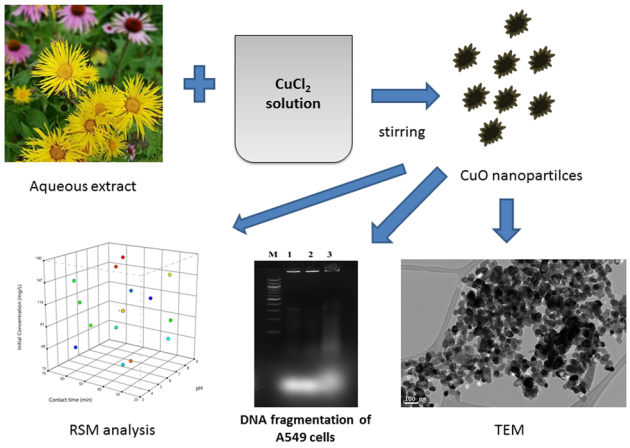

Graphical abstract

Keywords: *Inula*, CuO nanoparticles, antimicrobial, anticancer, antioxidant, adsorbent

1 Introduction

Metal nanoparticles (NPs), with their unique properties due to high surface area, are being heavily researched for their potential in various fields. Nanotechnology, particularly in food and agriculture, is a hot area with applications in areas such as food security, disease treatment, and environmental protection [1]. Bionanoscience,

* **Corresponding author: R. Lakshmipathy,** Directorate of Learning and Development, SRM Institute of Science and Technology, Kattankulathur, Tamil Nadu, 603203, India, e-mail: lakshmipathy.vit@gmail.com
Abdulaziz Alangari, Mourad A. M. Aboul-Soud: Department of Clinical Laboratory Sciences, College of Applied Medical Sciences, King Saud University, Riyadh, 11451, Saudi Arabia
Mohammed S. Alqahtani, Mudassar Shahid, Rabbani Syed: Department of Pharmaceutics, College of Pharmacy, King Saud University, P.O. Box 2457, Riyadh, 11451, Saudi Arabia
Jeevan Kumar Reddy Modigunta: Department of Polymer Science and Engineering, Chemical Industry Institute, Korea National University of Transportation, Chungju, 27469, Republic of Korea
Harshita Jaiswal: Department of Pharmacy, Parul University, Waghodia, Gujarat, 391760, India
Meenakshi Verma: University Centre for Research and Development, Chandigarh University, Mohali, Punjab, India

utilizing effective NPs, is also attracting attention for its uses in catalysis [2], cancer detection [3], and bioimaging [4].

Traditional methods for creating metal NPs offer precise control but often rely on harsh chemicals [5]. Biosynthesis presents a game-changing approach at the intersection of nanotechnology and biotechnology. This eco-friendly method utilizes biomolecules as safe and effective alternatives to chemical reductants, making it a highly attractive solution for sustainable NP production [6]. The biocompatible nature of these biomolecules adds another layer of advantage, promoting the development of NPs for applications in medicine and other fields [7,8]. Metallic NPs, including gold, silver, iron, zinc, and metal oxide NPs, have garnered attention for their potential in biomedical applications [9,10].

Copper (Cu) is a crucial metal used for the cross-linking of connective tissues, as well as for iron and lipid metabolism, but at high dose exposure it causes toxicity [11–13]. Owing to its antibacterial and antiviral properties, Cu and its compounds have been employed as disinfectants for ages [14]. Owing to its availability, Cu has been used to create copper oxide nanoparticles (CuO NPs). However, the challenges in the field of research include agglomeration and rapid oxidation. Like other metallic NPs, CuO NPs have a high surface-to-volume ratio that results in extremely high antibacterial capabilities [15,16].

CuO NPs were synthesized using the *Gloriosa superba* L. extract and have an aspect size of 5–10 nm [17]. Further, the CuO NPs exhibited superior antimicrobial efficiency toward Gram positive and Gram negative bacterial strains. Udayabhanu *et al.* synthesized CuO NPs of size around 6–8 nm and with a sponge-like structure using the *Tinospora cordifolia* water extract and successfully evaluated their photocatalytic, antioxidant, and antibacterial activities [18]. Velsankar *et al.* reported the biogenic synthesis of CuO NPs using the *Allium sativum* extract; the obtained CuO NPs were 20–40 nm in size and their antioxidant, antibacterial, and antilarvicidal activities were investigated [19]. Alhalili synthesized CuO NPs using *Eucalyptus globulus*, and the obtained NPs were spherical in shape with an average size of 88 nm [20]. The synthesized CuO NPs exhibited greater adsorption capacity toward methyl orange. CuO NPs were synthesized using the *Tamarindus indica* pulp extract, and the synthesized NPs were evaluated for their adsorption capacity toward As(III) ions [21]. The use of the mint leaf extract in the synthesis of CuO NPs was explored, and their efficiency in the removal of Pb ions from aqueous solution was investigated [22]. The CuO NPs exhibited a loading capacity of 88.8 mg g^{-1} toward Pb ions, and it was found to be higher than those of other two metal ions investigated in the study. Literature has revealed that the CuO NPs exhibited biological and environmental applications. However, the biosynthesized NPs were not simultaneously evaluated for their potential toward biological and environmental applications.

The genus *Inula*, belonging to the family *Asteraceae*, is widely distributed across Eurasia and Africa and is rich in pharmacologically active compounds such as terpenoids (including sesquiterpene lactones and dimers, diterpenes, and triterpenoids) [23–25]. Inula is recognized for its diverse range of biological activities, encompassing anticancer, antibacterial, hepatoprotective, cytotoxic, anti-neuroinflammatory, and anti-inflammatory properties [26,27]. Hence, the Inula extracts will be a useful source for the biosynthesis of NPs, and thus-synthesized NPs may have superior biological activities. To our knowledge, the synthesis and characterization of CuO NPs using the genus Inula have not been explored in previous studies. Therefore, the current investigation was undertaken to examine the potential ameliorative properties of CuO NPs synthesized from Inula for both anticancer and antibacterial activities and to further investigate the removal of Pb^{2+} ions from aqueous solution in a batch process.

2 Materials and methods

2.1 Chemicals

All solvents, standards, and reagents used were of analytical and HPLC grade. 1,1-Diphenyl picrylhydrazyl (DPPH) free radicals, hydrogen peroxide (H_2O_2), and sodium nitroprusside were purchased from Fluka Chemicals. Caspase-3 and -9 and p53 kits from MyBioSource (San Diego, California, United States), 3-(4,5-dimethylthiazolyl-2-yl)-2,5-diphenyl tetrazolium bromide (MTT), ethidium bromide, and agarose were obtained from Sigma Aldrich, St. Louis, MO, USA.

2.2 Collection of plant material and preparation of extract

Initially, 100 g of whole aerial part of plants of genus *Inula* was coarsely ground and subjected to boiling with 100 mL of deionized water with stirring at 60°C. After boiling the mixture for 60 min, a yellow solution was obtained containing the biomolecules of genus Inula. The extract was filtered with a Whatman filter paper and centrifuged at 12,000 rpm for 10 min. The supernatant was stored at 4°C, which was used as the reducing and capping agents.

2.3 Biosynthesis of CuO NPs

The biosynthesis of CuO NPs was carried out according to the method of Khodashenas and Ghorbani [15]. Briefly, about 45 mL of 1 mM $CuCl_2$ was taken in an amber-colored bottle and 45 mL of extract of Inula was added drop-by-drop under vigorous stirring with a magnetic stirrer. Upon addition of the extract, 1 mM NaOH was added gradually to the mixture containing the Cu precursor and extract, and the solution color turned black, indicating the formation of CuO particles. After complete addition of the solution, the mixture was stirred for another 120 min to ensure all of the Cu ions were converted to CuO particles. The mixture was centrifuged, and the solid black product obtained was dried in an oven at 100°C for 60 min and stored in air-tight containers for further use and characterization.

2.4 Characterization of CuO NPs

Initially, the confirmation of CuO NPs was achieved through visual analysis. The UV–visible spectrum of the colloidal solution containing CuO NPs was recorded using a Spectra MAX Plus (Molecular Devices, Sunnyvale, CA, USA) within the wavelength range of 200–700 nm. Fourier transform infrared (FTIR) spectroscopy was employed to identify the functional groups that might have played a role in the reduction and stability of the CuO NPs. Analysis was carried out between 4,000 and 400 cm^{-1} with 32 scans per min using the KBr pellet method. To assess the crystalline nature of the CuO NPs, X-ray diffraction (XRD) was conducted using the PANalytical Empyrean instrument in the 2θ range of 10–90. The morphology, size, and shape of the CuO NPs were determined using a JEM 2000EXII transmission electron microscopy (TEM) apparatus (M/s. JEOL, Switzerland). A particle size analyzer (Zetasizer Nano-ZS-90, Malvern software) was employed for particle size analysis at a scattering angle of 173° at 25°C coupled to a He–Ne laser.

2.5 Free-radical scavenging activity assay

The samples were evaluated using the DPPH assay following the prescribed methodology in the study of Abdel-Hameed *et al.* [28]. Specifically, 50 µL of each sample was combined with 150 µL of a 200 µM methanolic solution of DPPH and incubated at room temperature in the dark for 16 min. Subsequently, all samples were subjected to examination at the absorbance wavelength of 515 nm. The DPPH radical scavenging activity was determined using the following equation:

$$\text{Percent scavenging} = \left(\frac{\text{Absorbance control} - \text{Absorbance sample}}{\text{Absorbance control}}\right) \times 100. \quad (1)$$

The reaction was done in triplicate, and results are shown as % of inhibition of DPPH radicals.

2.6 H_2O_2 radical scavenging assay

A 20 mM H_2O_2 pH 7.4 solution was prepared in phosphate buffer. To generate various concentrations, 2 mL of H_2O_2 solution in PBS was added to 1 mL of both the samples and the standard. Following a 10-min incubation period, the absorbance at 230 nm was measured [29].

2.7 Nitric oxide (NO) scavenging activity

The NO-scavenging capacity of the extracts was assessed using previously established methods with slight modifications. The quantity of extract required to neutralize 50% of the NO radicals generated by sodium nitroprusside was utilized to express the activity as a percentage of inhibition, and the IC_{50} value was determined.

2.8 Lipid peroxidation and antioxidant enzyme assays for CuO NP-treated cells

Lipid peroxidation was assessed by quantifying malondialdehyde (MDA) [30]. In cultured A549 cells, pre-treatment with CuO NPs was carried out for 60 min, followed by exposure to 100 µM H_2O_2 for an additional 60 min. The A549 cells, pre-treated with CuO NPs, were then lysed using a lysis buffer. The activity of superoxide dismutase (SOD) was determined using the nitroblue tetrazolium method [31]. Catalase (CAT) and glutathione peroxidase (GPX) activities were assessed according to previously established protocols [32,33].

2.9 Cytotoxicity and morphological changes in A549 cells

The cytotoxic effects of CuO NPs were assessed by observing morphological changes in A549 cells. The treatment dose, presumed to correspond to the IC_{50} value of CuO NPs

(15.00 µg/mL), was determined using phase-contrast microscopy. Morphological characteristics indicative of cytotoxicity, such as membrane blebbing, cell shrinkage, and necrosis, were identified during the observation.

2.10 Caspase-3, caspase-9, and p53 assays by ELISA

Caspase activity was determined through the use of caspase-3, caspase-9, and p53 ELISA kits following the manufacturer's protocol. Briefly, 50,000 A549 cells were seeded into each well of a 96-well plate and incubated in a humidified incubator at 37°C with 5% CO_2 for 24 h. The 96-well plate, containing both CuO NPs-treated and control cells, was then allowed to equilibrate at room temperature. Caspase-3 and -9 reagents were added to each well of the plate, containing 100 µL of culture media (CuO NP-treated and control). The plate was covered entirely, and the mixture was agitated at 500 rpm for 30 s. After a 30 min incubation at room temperature, the transmittance at 405 nm was measured using an ELISA reader.

2.11 DNA fragmentation induced by CuO NPs

A549 cell line cells were treated with CuO NPs at IC_{50} and 2× IC_{50} concentrations to induce apoptosis in order to study DNA fragmentation. In accordance with the manufacturer's recommendations, DNA purification kits were used to extract the DNA (Thermo Fisher Scientific, CA, USA). Following quantification, 2 µg of each DNA sample was loaded for electrophoresis on a 1.5% agarose gel, and the gel was stained with ethidium bromide before being photographed under UV light.

2.12 Antimicrobial activity

The antimicrobial activity was determined according to a previously described protocol [34]. Briefly, the agar diffusion method was used to analyze it. Four bacterial strains, including both Gram positive *Bacillus subtilis* (*B. subtilis*) and *Staphylococcus aureus* (*S. aureus*) and Gram negative *Escherichia coli* (*E. coli*) *and Klebsiella pneumoniae* (*K. pneumoniae*), were subcultured in fresh Muller Hinton broth. The stock culture was prepared for each strain by a calorimetric method using the McFarland standard. Ampicillin (10 µg/mL) was used as the positive control. Muller Hinton agar (HiMedia, India) plates were streaked with each bacterial strain. Using a 6 mm borer, three wells were bored. Each well was filled with 100 µl of In-NP, ampicillin, or culture media as a negative control. All the plates were dried for 15 min and incubated for 24 h. All the experiments were done in triplicate. The zone of inhibition (ZOI) was calculated by taking the mean of ZOI of each plate.

2.13 Cytokine assay

Cells were cultured with different concentrations of CuO NPs at 37°C for 24 h. Following the culture period, the supernatant was collected, and the levels of cytokines, TNF-α and IL-6, were measured using ELISA kits in accordance with the manufacturer's instructions.

2.14 Statistical analysis

The results for antimicrobial assessment of CuO NPs were analyzed in Prism software using the Student's t-test, and p-value <0.05 was considered statistically significant.

2.15 Response surface methodology (RSM)

The central composite design (CCD) is a widely employed second-order polynomial design within RSM, particularly valuable for investigating the collective impact of operational variables on the efficiency of metal adsorption. An essential advantage of CCD in a step-by-step experimental process is its capacity to yield meaningful results with a minimal number of designated points, providing a practical framework for data fitting. This approach is instrumental in gaining insights that can be effectively applied to either select or enhance the proposed model. In this study, a full factorial design consisting of 20 runs was conducted, and the main factors, symbols, and their values are detailed in Table 1. The CCD was developed using Design-Expert v13 software.

3 Results and discussion

3.1 UV–visible analysis

The synthesized CuO NPs were analyzed with a UV–visible spectrophotometer, and the absorption spectrum was

Table 1: Independent variables and their levels and symbols for the optimization of variables

Variables	Symbol	Levels		
		−1	**0**	**+1**
pH	*A*	4	6	8
Contact time	*B*	30	45	60
Initial concentration	*C*	50	100	150

obtained between 200 and 700 nm. The UV–visible absorption spectrum is depicted in Figure 1, and it is observed that the spectrum contains three major absorption peaks at 279, 300, and 346 nm. The absorption peaks at 279 and 300 nm correspond to the capping and stabilizing agents that are bound to the CuO NPs. The absorption peak at 346 nm corresponds to the surface plasmon resonance of the excitation of the CuO NP semiconductor. Similar results were reported by Aziz *et al.* for the CuO synthesized from mint leaves [35]. The optical band energy of the CuO NPs was calculated with the Tauc plot and was found to be 4.07 eV, which is high compared to that of the bulk CuO material.

3.2 FTIR analysis

FTIR analysis is majorly employed in identifying the organic functional groups; however, it is also helpful in identifying the metal oxide bonds which are usually seen in fingerprint regions. In this study, a CuO NP solution was subjected to FTIR, and the spectrum is displayed in Figure 2. The broad bands at 3,305 cm^{-1} correspond to the stretching vibrations of O–H functional groups, and the band at 1,636 cm^{-1} corresponds to the asymmetric stretching vibrations of O–H groups [22]. A small peak at 1,016 cm^{-1} corresponds to the bending vibrations of the R–OH groups on the surface of the CuO NPs. The Cu–O bands are generally observed around 600 cm^{-1}, and a sharp band around 600 cm^{-1} corresponds to the Cu–O bond vibration, which confirms the formation of Cu–O. In this study, the CuO NP solution was subjected to FTIR, and due to the solvent, the major functional molecules present on the CuO NPs are overshadowed by the solvent intense peaks. The peaks observed between 2,400 and 2,000 cm^{-1} are due to noise arising from liquid solvents. Very similar peaks and results were obtained for the CuO NPs synthesized using *Aerva lanata* [36].

3.3 XRD analysis

XRD analysis was carried out to understand the synthesized CuO NPs' crystallinity and phase (Figure 3). The XRD pattern depicted several fairly sharp peaks, indicating the crystallinity of the synthesized CuO NPs. The diffraction peaks at 32.4°, 35.5°, 38.7°, 48.7°, 53.4°, 58.3°, 61.5°, 66.2°, 68.0°, 72.4°, and 75.2° correspond to 110, 111, 111, 112, 020, 202, 113, 311, and 113 planes of monoclinic CuO (JCPDS No. 45-0937). The diffraction peaks were very distinct and

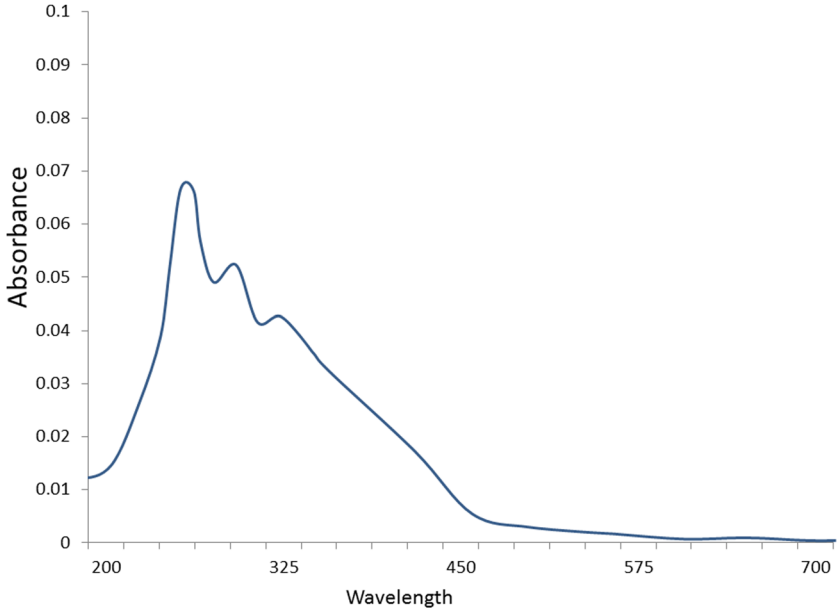

Figure 1: UV–visible spectrum of CuO NPs.

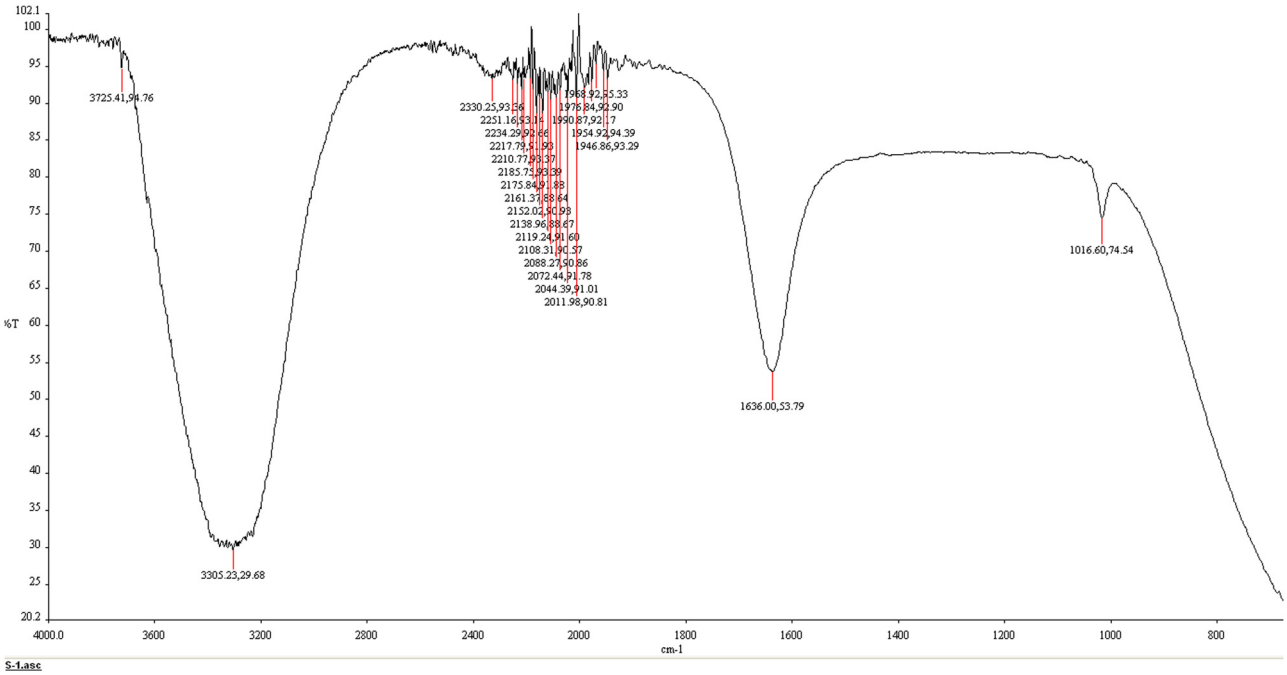

Figure 2: FTIR spectrum of CuO NPs synthesized using the genus *Inula* extract.

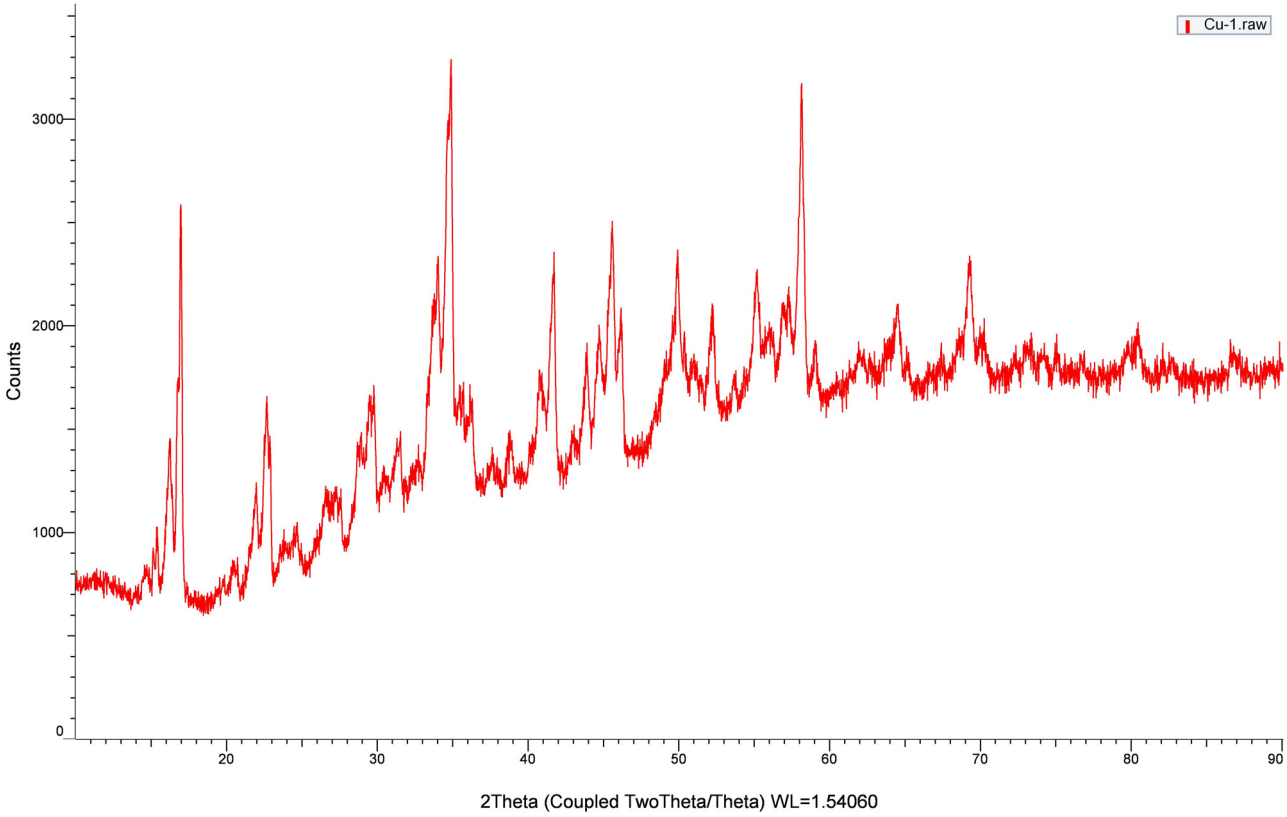

Figure 3: XRD pattern of CuO NPs synthesized using the genus *Inula* extract.

slightly broad, depicting the nano size level of CuO. All the diffraction peaks correspond to the CuO monoclinic phase, and additional peaks are noticed in the patterns. Similar results were reported for the CuO NPs synthesized using the *C. gigantea* leaf extract [37].

3.4 Particle size and zeta potential analyses

The log-normal distribution is widely used for the simplified representation of particle size distribution. The hydrodynamic diameter and polydispersity index of the synthesized CuO were found to be less than 100 nm, confirming the nanosized CuO particles (Figure 4). The large size distribution of the particles observed is due to small amounts of large aggregates in addition to the distinctly smaller size CuO NPs, and at times the dust particles also influence the size distribution, and these are considered to be the pitfalls of the dynamic light scattering technique [38]. Additionally, the zeta potential was measured as negative mV, suggesting the stability of CuO NPs.

3.5 TEM and energy-dispersive X-ray spectrometry (EDX) analyses

TEM was used to understand the morphology of the newly developed CuO NPs. The TEM image (Figure 5) shows the formation of spherical CuO NPs with an average size of 20 nm. The CuO NPs are clearly distributed with less agglomeration. The spherical shape and less agglomeration are due to the biomolecules of genus *Inula* capping onto the CuO NPs, restricting their size and shape. EDX investigations were performed for the CuO NPs in order to confirm

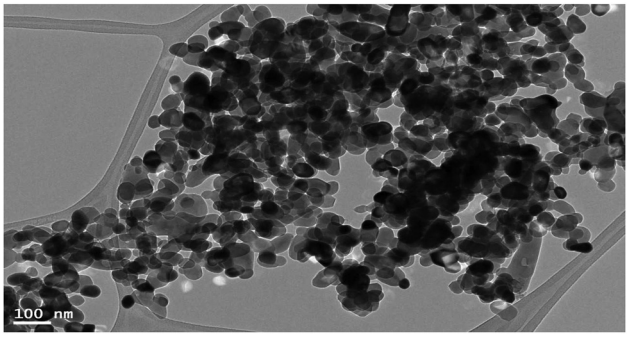

Figure 5: TEM image of CuO NPs synthesized using the genus *Inula* extract.

the CuO NP formation and identify the purity of the CuO NPs. The EDX patterns (Figure S1) displayed peaks for Cu and O atoms, and no other peaks were observed. This observation revealed that the CuO NPs were pure and no impurities were present.

3.6 Free-radical scavenging activity: Antioxidant assays

Oxidative stress and the presence of reactive oxygen species have been implicated in various human diseases, including carcinoma, arteriosclerosis, inflammatory disorders, and the aging process [39]. There is a growing interest in identifying naturally occurring antioxidants for applications in foods, cosmetics, or medicinal materials, aiming to replace synthetic antioxidants that are facing restrictions due to their carcinogenic properties [30]. Dietary and herbal formulations with free-radical scavenging potential have gained significance in the treatment of chronic diseases. Numerous studies have established a connection between the antioxidant activities of fruits, vegetables,

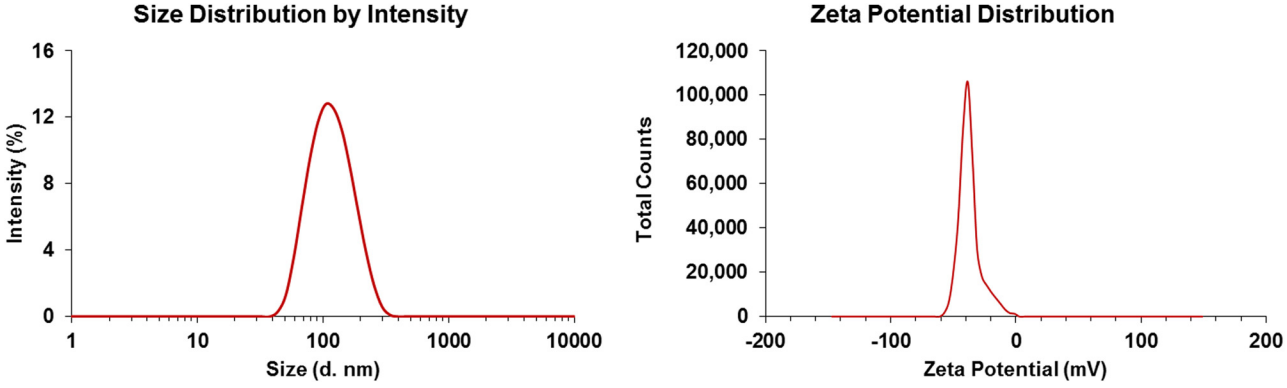

Figure 4: Particle size distribution and zeta potential analysis of CuO NPs.

and medicinal herbs and their phenolic compound content [39–42]. The antioxidant properties of aqueous extracts used for CuO NPs synthesis were chemically estimated using the DPPH radical scavenging activity at an IC_{50} value of 22.16 µg/mL. The IC_{50} value was nearly equal to one third of standard ascorbic acid. The determination of NO activity using the sodium nitroprusside method showed that CuO NPs had high antioxidant capacity with IC_{50} values of 25.1 ± 4.25 and 14.26 ± 0.98 µg/mL for hydrogen peroxidase (Figure 6). The findings of this study were consistent with previous research on the antioxidant properties of some lotus species [43,44].

3.7 Lipid peroxidation and antioxidant enzyme assays

To assess the homeostasis of antioxidant defense mechanisms, we conducted an analysis of endogenous antioxidants such as SOD, CAT, and GPX. Following treatment with CuO NPs at a concentration of 30 µg/mL, the cells demonstrated a noteworthy ($p < 0.05$) alteration in antioxidant levels. Specifically, there was a significant decrease observed in the levels of SOD, CAT, and GPX by 52.2%, 42.34%, and 42.5%, respectively (refer to Figure 7a–c). Conversely, A549 cells treated with CuO NPs at a concentration of 30 µg/mL exhibited a significant ($p < 0.05$) increase in MDA content (Figure 7d). Heat maps represent the fold change in enzyme activities and MDA levels compared to the control group, with green indicating a decrease, red an increase, and black no change. Significant differences from the control group were assessed using analysis of variance (ANOVA) with $^{*}p < 0.05$, $^{**}p < 0.01$, $^{***}p < 0.001$, and ns indicating not significant. Each bar represents the mean ± SEM of three independent experiments. This elevation in MDA content suggests oxidative stress-induced lipid peroxidation, leading to the dysregulation of overall lipid metabolism and associated mechanisms.

3.8 Cytotoxic effect of CuO NPs on A549 cells by cell viability assay

In comparison to A549 cell lines, the MTT assays showed a concentration-dependent reduction in viability for CuO NPs (Figure 8). The IC_{50} value for CuO NPs in A549 cells was determined to be 15.36 µg/mL. According to the MTT assay results, CuO NPs had encouraging anticancer activity against lung cancer cell lines, most probably due to the existence of antioxidant phytoconstituents, and previous research has suggested that CuO NPs may be used as an effective drug booster in the treatment of non-small-cell

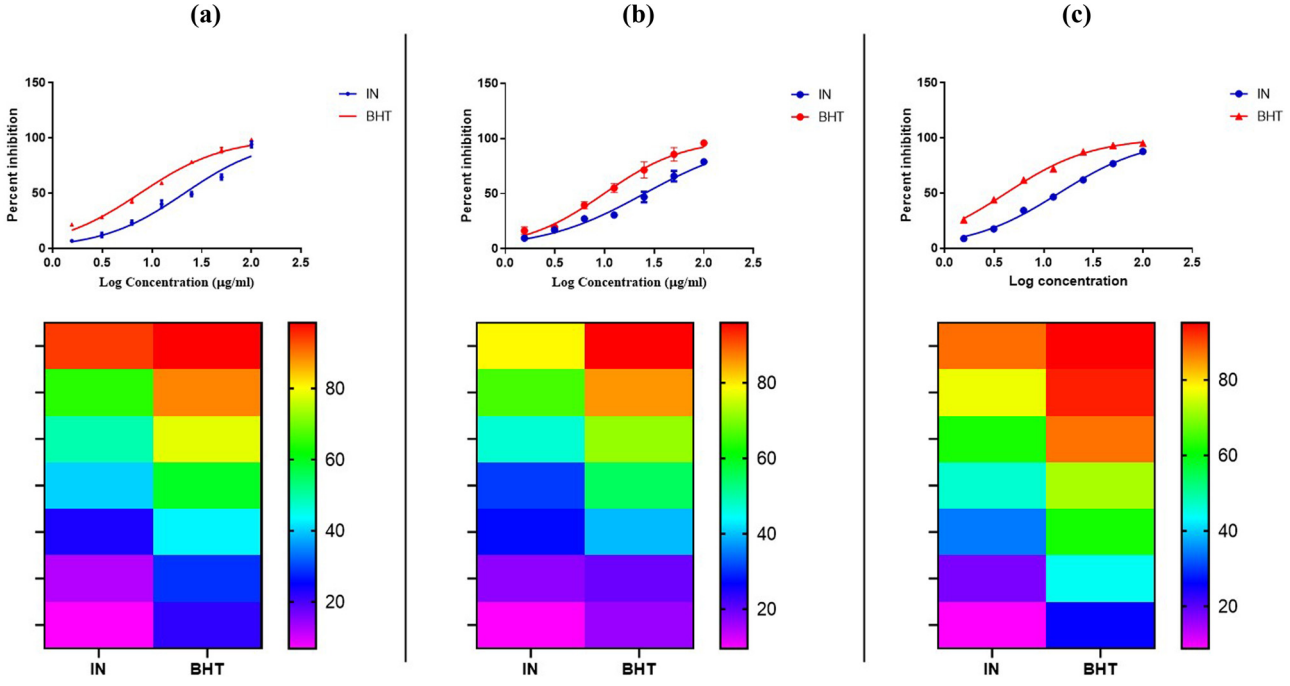

Figure 6: Panels (a)–(c) depicting the antioxidant capacity of CuO NPs in comparison to butylated hydroxytoluene across a range of concentrations. (a) DPPH, (b) NO, and (c) H_2O_2. Values are expressed as mean ± SD ($n = 3$).

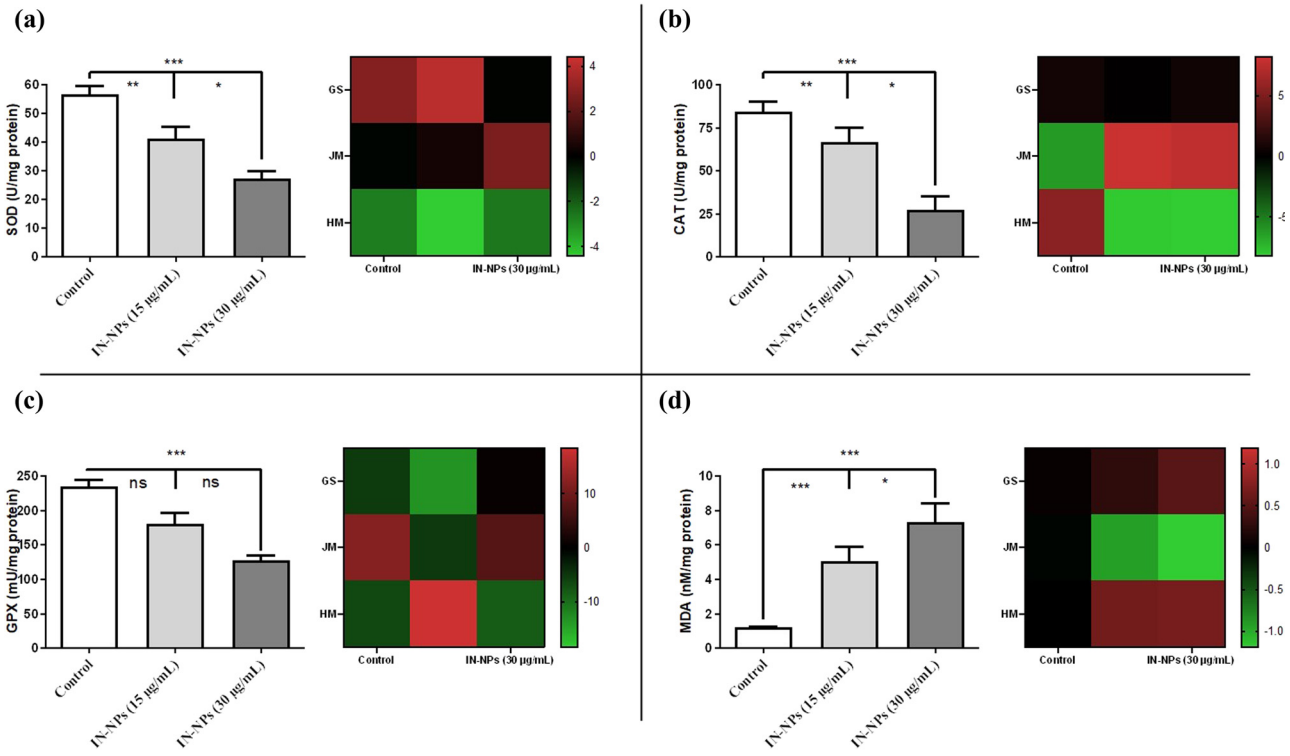

Figure 7: Effects of CuO NPs on antioxidant enzyme activities and lipid peroxidation levels. The bar graphs and corresponding heatmaps show the activities of (a) SOD, (b) CAT, and (c) GPX, along with (d) levels of MDA in the presence of increasing concentrations of CuO NPs.

lung cancer [45,46]. Cu NPs have been studied extensively due to their unique properties and potential applications in various fields including biomedicine. However, the same properties that make CuNPs attractive for applications like antimicrobial agents, drug delivery, and imaging also necessitate a thorough understanding of their potential cytotoxic effects [47].

3.9 Activation of apoptotic regulatory genes (caspase-3, caspase-9, and p53) by CuO NPs

Apoptosis is a sort of induction process in which intracellular components are disassembled while nearby cells are

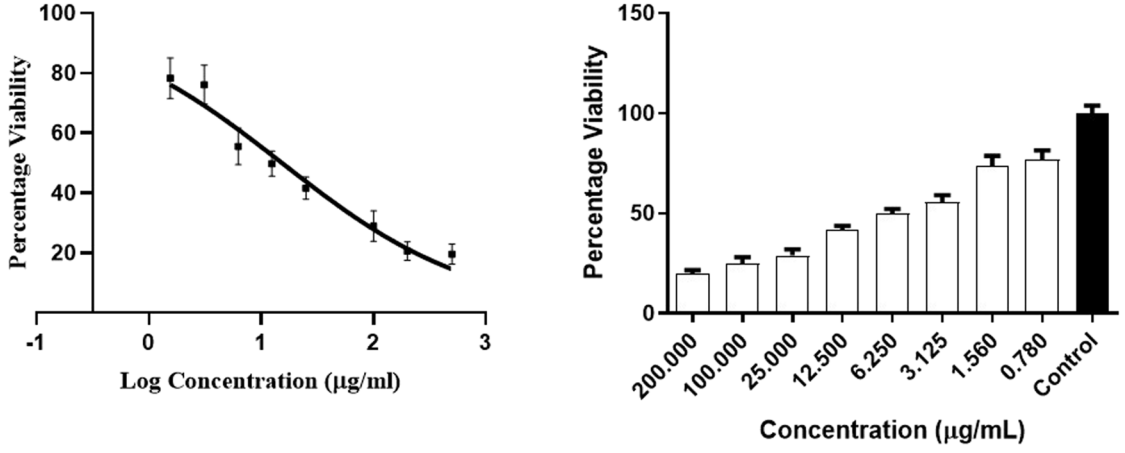

Figure 8: Dose response cure for cytotoxicity of CuO NPs after 24 h incubation with A549 cells at concentrations of 0.78 to 200 µg/mL. Left graph: Dose–response curve, showing the percentage of cell viability as a function of logarithm of the concentration (µg/mL) of the substance. Right graph: Bar chart showing the percentage of cell viability at specific concentrations of the substance, which are not log-transformed.

not injured or inflamed [48]. Caspase-3 and -9 and p53 activation is primarily responsible for tumor cell apoptosis. To confirm apoptosis, an increase in caspase-3 and -9 and p53 production in CuO NP-treated A549 cells was done, especially in comparison to the untreated group in this study. Once A549 cells were exposed to CuO NPs, their caspase-3 and -9 and p53 activity increased up to fourfold compared to that of control (untreated) cells (Figure 9). The increased effectiveness of CuO NPs indicates a possible cause of caspase activation in cancer cells.

3.10 DNA fragmentation analysis

Apoptosis is distinguished by DNA internucleosomal rupture, cell membrane blebbing, nuclear chromatin condensation in the nuclear periphery, and the formation of apoptotic condensed nuclear bodies. A549 cells were treated with different concentrations of CuO NPs to verify apoptosis induction, and DNA was isolated and analyzed using agarose gel electrophoresis. A549 cells treated with CuO NPs (15 and 30 µg/mL; IC_{50} and 2× IC_{50}) for 24 h showed significant internucleosomal fragmentation (Figure 10). DNA strand breaks were found to be present during apoptosis, and scratches in

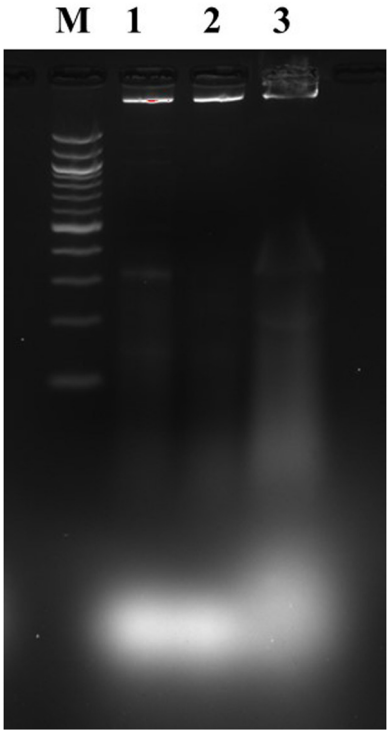

Figure 10: Agarose gel electrophoresis of DNA samples (M, marker 100 bp; 1 = CuO NPs, 15 µg/mL; 2 = IN-Control; 3 = CuO NPs, 30 µg/mL).

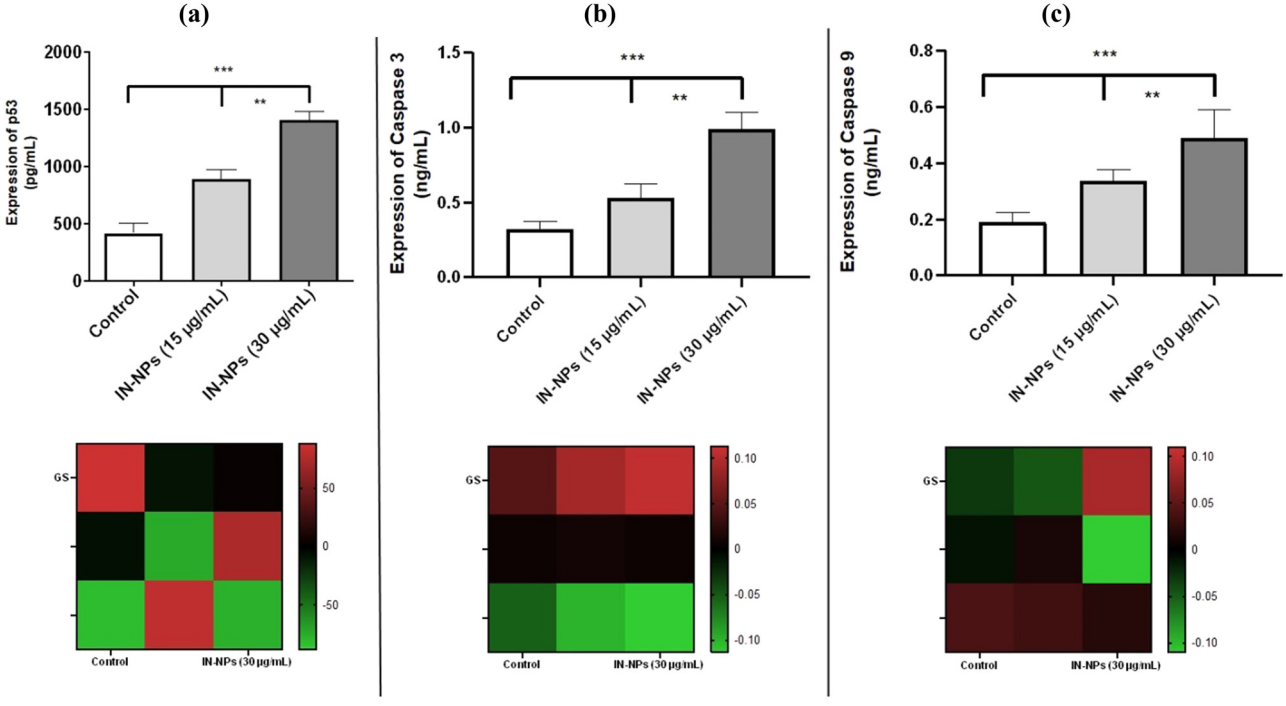

Figure 9: Bar graphs (a)–(c) and the corresponding heat maps (below each graph), representing the expression levels of p53, caspase-3, and caspase-9, respectively, in response to varying concentrations of CuO NPs.

DNA molecules could be detected using a DNA fragmentation assay. Apoptosis is well known to be engaged in the stimulation of endonucleases, which ultimately results in DNA fragmentation, which can be seen *via* electrophoretic investigation [49]. In this study, agarose gel electrophoretic findings show that internucleosomal DNA fragmentation aided the steady progress of apoptosis in CuO NP-treated A549 cells. Lane M contains a DNA ladder used as a molecular-weight marker. Lanes 1 and 2 show a sample with high-molecular-weight DNA with no significant fragmentation. Lane 3 displays samples with extensive DNA fragmentation, as evidenced by the smeared pattern rather than discrete bands, which is indicative of DNA degradation. This fragmentation pattern is typically observed in samples undergoing apoptosis or those treated with nucleases.

3.11 Antimicrobial activity

Gram-positive strains *B. subtilis* and *S. aureus* showed susceptibility toward CuO NPs with ZOIs of 25.4 ± 3.12 and 24.2 ± 1.12 mm with *p*-values 0.012 and 0.020, respectively, compared to ampicillin, whereas Gram-negative strains *E. coli* and *K. pneumoniae* showed resistance toward CuO NPs with ZOIs of 17.27 ± 0.82 and 23.63 ± 2.32 mm with *p*-values 0.08 and 0.91, respectively, compared to standard ampicillin, and the results are shown in Table 2. The antimicrobial activity of *Inula* species is thought to be due to the presence of a number of compounds, including flavonoids, terpenes, and sesquiterpenes. Flavonoids are plant pigments that have antioxidant and anti-inflammatory properties [50]. A number of studies have shown that *Inula* extracts and essential oils have antimicrobial activity against a variety of bacteria and antifungal activity against *Candida albicans* [50]. The antimicrobial activity of the formulation is thought to be due to a number of factors, including the ability of *Inula* compounds to disrupt the cell membrane of bacteria, inhibit protein synthesis, and damage DNA.

Table 2: Antimicrobial efficacy of CuO NPs in comparison to standard ampicillin

Microorganism	ZOI (mm) expressed in mean ± SD, n = 3		
	ZOI of CuO NPs (mm)	ZOI of ampicillin (mm)	ZOI of blank (mm)
B. subtilis	25.4 ± 3.12	20.97 ± 2.1	7.1 ± 1.2
S. aureus	24.2 ± 1.12	19.03 ± 1.22	6.87 ± 2.17
E. coli	17.27 ± 0.82	21.43 ± 3.12	7.63 ± 0.91
K. pneumoniae	23.63 ± 2.32	23.9 ± 3.2	7.5 ± 1.02

Table 3: Experimental and predicted values for the removal of Pb^{2+} ions by CuO NPs

Run No.	pH	Contact time	Initial concentration	Exp (%)	Pre (%)
1	9	45	100	11.50	3.81
2	4	60	50	52.30	56.33
3	4	30	150	14.90	16.54
4	6	45	100	82.40	83.39
5	6	45	15	96.20	86.19
6	8	30	50	40.60	49.14
7	6	45	100	82.40	83.39
8	8	60	50	47.50	51.78
9	4	60	150	63.00	60.38
10	6	20	100	53.20	45.72
11	6	70	100	85.50	84.46
12	3	45	100	10.40	7.57
13	6	45	100	83.10	83.39
14	8	30	100	14.20	16.09
15	6	45	100	83.20	83.39
16	6	45	100	82.90	83.39
17	6	45	100	83.00	83.39
18	4	30	50	22.50	27.64
19	8	60	150	33.10	33.88
20	6	45	180	61.30	63.35

3.12 RSM

In this study, three independent variables – pH, contact time, and initial concentration – were selected, and a 20-

Table 4: ANOVA of Pb^{2+} ion removal by CuO NPs

Source	Sum of squares	df	Mean square	*F*-value	*p*-value
Model	15965.08	9	1773.90	46.85	<0.0001
A – pH	19.59	1	19.59	0.5175	0.4884
B – Contact time	1830.74	1	1830.74	48.35	<0.0001
C – Initial concentration	704.81	1	704.81	18.61	0.0015
AB	339.30	1	339.30	8.96	0.0135
AC	240.90	1	240.90	6.36	0.0303
BC	114.76	1	114.76	3.03	0.1123
A^2	12262.11	1	12262.11	323.85	<0.0001
B^2	613.23	1	613.23	16.20	0.0024
C^2	148.90	1	148.90	3.93	0.0755
Residual	378.63	10	37.86		
Lack-of-fit	378.02	5	75.60		
Pure error	0.6133	5	0.1227		
Cor total	16343.71	19			
R^2	0.9768				
Adjusted R^2	0.9560				
Predicted R^2	0.8184				
Adeq precision	18.9332				

run CCD was employed, consisting of 8 cubic points, 6 axial points, and 6 center points within a cube. The predicted and experimental design matrices and ANOVA for the removal of Pb^{2+} ions by CuO NPs are presented in , respectively. A quadratic model was established using Design-Expert v13, and the second-order polynomial equation for the removal is expressed in the following equation:

$$\% \text{ Removal} = 83.39 + 1.25A + 11.62B - 7.25C - 34.53A^2 - 6.59B^2 - 3.30C^2 - 6.51AB - 5.49AC + 3.79BC. \quad (2)$$

The quadratic equations mentioned above are characterized by coefficients that signify their intensity. Additionally, the sign of these coefficients provides insights into whether a specific variable exerts a positive or negative influence on the response. A positive coefficient indicates that increasing the level of a factor enhances the response, while a negative coefficient suggests that increasing the level of a factor impedes the response. The model includes three primary effects, three two-factor interaction effects, and three curvature-related effects. Eq. (2) visually illustrates the independent

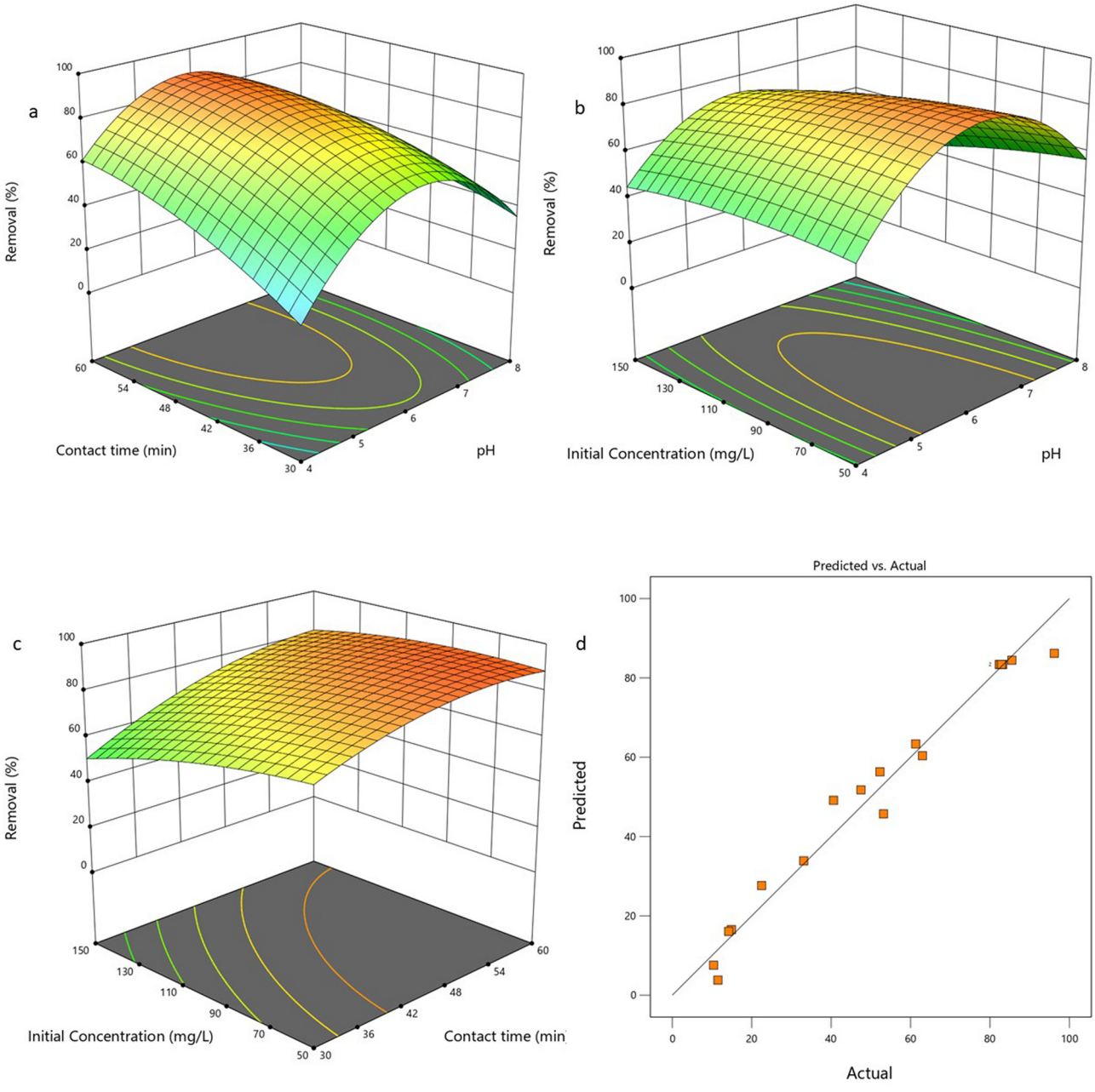

Figure 11: 3D surface plots of (a) pH *vs* contact time, (b) pH *vs* initial concentration, (c) contact time *vs* initial concentration, and (d) probability plot of actual *vs* predicted.

Table 5: Loading capacity comparison of CuO NPs

S. No	CuO NPs synthesis method	Loading capacity (mg g^{-1})	Ref.
1	Mint leaf extract	88.8	[22]
2	Coprecipitation	97.0	[51]
3	Magnetron sputtering	37.0	[52]
4	*In situ* soft chemical synthesis	3.31	[53]
5	Genus *Inula* extract	124.7	This study

variables and their impact on the responses of the experiment. Furthermore, the close correlation between the experimental and predicted values (Table 3) suggests the applicability and improved responses of the experiments.

The ANOVA results for Pb^{2+} ion removal by CuO NPs are summarized in Table 4. The perfection and exactness of the present model can be understood from the *p*-values, and in this study the *p*-value was <0.0001, which is statistically significant. Further, the reliability and applicability of a model are supported by the *F*-value, which was found to be 46.85 herein, and the higher *F*-value indicated that the model is more reliable, and there is only 0.01% chance that the *F*-value of this large can occur due to noise. The lack-of-fit *F*-value was determined to be >0.1, indicating the absence of systematic variation encountered in the hypothesized model. It is crucial to validate and confirm that the adopted model provides a satisfactory approximation, and this was verified by examining the probability plot of actual *versus* predicted values to assess the accuracy. Figure 11d illustrates the probability plot, revealing no significant deviation. While a slight scattering of points is observed in the plot, it can be assumed that the data distribution is normal, with no need for response transformation or correction, as the points align along a straight line. The correlation coefficients were found to be 0.976, and the adjusted and predicted R^2 were found to be 0.956 and 0.818, respectively, which support the applicability of the model. The adequate precision was noted to be 18.9, suggesting that adequate signals are obtained for the developed model.

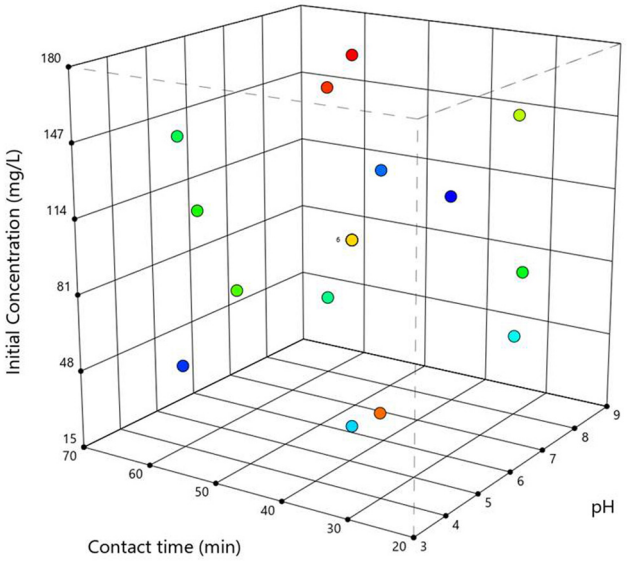

Figure 12: Distribution of points of independent variables for the removal of Pb^{2+} ions by CuO NPs.

The 3D surface plots provide a visual representation of the interactions of independent variables and their influence on the removal percentage of Pb^{2+} ions by CuO NPs. The 3D plots obtained in this study are presented in Figure 11a–c. The interaction of pH and contact time and their influence on removal of Pb^{2+} ions are shown in Figure 11a. It can be observed that the maximum removal efficiency is achieved at pH 6 with increasing contact time. The removal efficiencies were observed to be low at pH 4 and 8 and at lower contact times, and this can be explained as that at low pH the hydronium ions compete for the active sites on the CuO NPs and thus the removal efficiencies are low. At pH 6, the competition exhibited by the hydronium ions are minimal due to lesser concentrations, thus maximizing the efficiency. Furthermore, a higher contact time provides suffice time for the Pb^{2+} ions to interact and bind to the surface of CuO NPs. The interaction between pH and initial concentrations indicates that the optimal pH should be 6 and low initial concentrations result in higher removal efficiencies. With an increase in the concentration of Pb^{2+} ions, the efficiencies decrease, and this is due to the exhaustion of the surface active sites. Similarly, in the case of contact time and initial concentrations, higher contact times with lower initial concentrations are preferred for optimal removal of Pb^{2+} ions by CuO NPs. The loading capacity of CuO NPs toward Pb^{2+} ions was found to be 124.7 mg g^{-1} in the preliminary investigations. The loading capacity exhibited in this study is high compared to other CuO NPs synthesized *via* different extracts and methods (Table 5). A 3D cube distribution of points at various values of independent variables is presented in Figure 12. It is observed that a maximum of six points are concentrated at pH 6, a contact time of 45 min,

and an initial concentration of 100 mg L^{-1}, suggesting the optimal conditions for the Pb^{2+} ions. A systematic investigation will reveal the mechanism and nature of adsorption of Pb^{2+} ions onto CuO NPs.

4 Conclusions

The present study investigated the biosynthesis of CuO NPs using the aqueous extract of genus *Inula* at low temperatures. The obtained CuO NPs were characterized by UV–visible, FTIR, XRD, and TEM techniques and confirmed their formation. The obtained CuO NPs were found to be around 20 nm with a spherical shape. Applications of CuO NPs exhibited enhanced gene expression toward apoptotic genes and induced apoptosis *via* up- and downregulation. The CuO NPs also exhibited excellent antimicrobial properties toward the tested pathogens. RSM-based CCD was developed to optimize and assess the ability of CuO NPs to adsorb Pb^{2+} ions from aqueous solution. The developed model was found to be reliable and significant with a p-value <0.0001. These results conclude that the genus *Inula*-based CuO NPs exhibit excellent biological activity and adsorption ability. Further investigations are required to establish the real-time application *via* pharmaceutical formulations and in wastewater treatment.

Acknowledgments: The authors extend their appreciation to the Researchers Supporting Project number (RSPD2024R1005), King Saud University, Riyadh, Saudi Arabia, for funding this work.

Funding information: This research was funded by the Researchers Supporting Project number (RSPD2024R1005), King Saud University, Riyadh, Saudi Arabia.

Author contributions: All authors have accepted responsibility for the entire content of this manuscript and approved its submission.

Conflict of interest: The authors state no conflict of interest.

Data availability statement: All data generated or analyzed during this study are included in this published article (and its supplementary information files).

References

[1] Mody V, Siwale R, Singh A, Mody H. Introduction to metallic nanoparticles. J Pharm Bioall Sci. 2010;2:282.

[2] Hashmi ASK, Hutchings GJ. Gold catalysis. Angew Chem Int Ed. 2006;45:7896–7936.

[3] Zhang Y, Li M, Gao X, Chen Y, Liu T. Nanotechnology in cancer diagnosis: progress, challenges and opportunities. J Hematol Oncol. 2019;12:137.

[4] Han X, Xu K, Taratula O, Farsad K. Applications of nanoparticles in biomedical imaging. Nanoscale. 2019;11:799–819.

[5] Umer H, Ramzan A, Shakil S, Azeem S. A numerical study on thin film flow and heat transfer enhancement for copper nanoparticles dispersed in ethylene glycol. Rev Adv Mater Sci. 2023;62(1):20220320.

[6] Nzilu DM, Madivoli ES, Makhanu DS. Green synthesis of copper oxide nanoparticles and its efficiency in degradation of rifampicin antibiotic. Sci Rep. 2023;13:14030.

[7] Singh J, Dutta T, Kim KH, Rawat M, Samddar P, Kumar P. 'Green' synthesis of metals and their oxide nanoparticles: applications for environmental remediation. J Nanobiotechnol. 2018;16:84.

[8] Khan ZUH, Khan A, Chen Y, Shah NS, Muhammad N, Khan AU, et al. Biomedical applications of green synthesized Nobel metal nanoparticles. J Photochem Photobiol B: Biol. 2017;173:150–64.

[9] Iravani S. Green synthesis of metal nanoparticles using plants. Green Chem. 2011;13:2638.

[10] Vijayaram S, Razafindralambo H, Sun YZ, Vasantharaj S, Ghafarifarsani H, Hoseinifar SH, et al. Applications of green synthesized metal nanoparticles — a review. Biol Trace Elem Res. 2024;202:360–86.

[11] Bhattacharya PT, Misra SR, Hussain M. Nutritional aspects of essential trace elements in oral health and disease: an extensive review. Scientifica. 2016;2016:5464373.

[12] Alarifi S, Ali D, Verma A, Alakhtani S, Ali BA. Cytotoxicity and genotoxicity of copper oxide nanoparticles in human skin keratinocytes cells. Int J Toxicol. 2013;32:296–307.

[13] Moschini E, Gualtieri M, Colombo M, Fascio U, Camatini M, Mantecca P. The modality of cell–particle interactions drives the toxicity of nanosized CuO and TiO2 in human alveolar epithelial cells. Toxicol Lett. 2013;222:102–16.

[14] Grass G, Rensing C, Solioz M. Metallic copper as an antimicrobial surface. Appl Environ Microbiol. 2011;77:1541–7.

[15] Khodashenas B, Ghorbani HR. Synthesis of copper nanoparticles: An overview of the various methods. Korean J Chem Eng. 2014;31:1105–9.

[16] Ma X, Zhou S, Xu X, Du Q. Copper-containing nanoparticles: Mechanism of antimicrobial effect and application in dentistry-a narrative review. Front Surg. 2022;9:905892.

[17] Naika HR, Lingaraju K, Manjunath K, Kumar D, Nagaraju G, Suresh D, et al. Green synthesis of CuO nanoparticles using Gloriosa superba L. extract and their antibacterial activity. J Taibah Univ Sci. 2015;9(1):7–12.

[18] Udayabhanu PC, Nethravathi MA, Kumar DP, Suresh K, Lingaraju H, Rajanaika H, et al. Tinospora cordifolia mediated facile green synthesis of cupric oxide nanoparticles and their photocatalytic, antioxidant and antibacterial properties. Mater Sci Semicond Process. 2015;33:81–8.

[19] Velsankar K, Kumar ARM, Preethi R, Muthulakshmi V, Sudhahar S. Green synthesis of CuO nanoparticles via Allium sativum extract and its characterizations on antimicrobial, antioxidant, antilarvicidal activities. J Env Chem Eng. 2020;8(5):104123.

[20] Alhalili Z. Green synthesis of copper oxide nanoparticles CuO NPs from eucalyptus globoulus leaf extract: Adsorption and design of experiments. Arab J Chem. 2022;15(5):103739.

[21] Singh DK, Verma DK, Singh Y, Hasan SH. Preparation of CuO nanoparticles using Tamarindus indica pulp extract for removal of As(III): Optimization of adsorption process by ANN-GA. J Env Chem Eng. 2017;5(1):1302–18.
[22] Mahmoud AED, Al-Qahtani KM, Alflaij SO. Green copper oxide nanoparticles for lead, nickel, and cadmium removal from contaminated water. Sci Rep. 2021;11:12547.
[23] Tavares WR, Seca AML, Inula L. Secondary metabolites against oxidative stress-related human diseases. Antiox. 2019;8:122.
[24] Seca AML, Grigore A, Pinto DCGA, Silva AMS. The genus inula and their metabolites: from ethnopharmacological to medicinal uses. J Ethnopharmacol. 2014;154:286–310.
[25] Seca AML, Pinto DCGA, Silva AMS. Metabolomic profile of the genus inula. Chem Biodivers. 2015;12:859–906.
[26] Khan AL, Hussain J, Hamayun M, Gilani SA, Ahmad S, Rehman G, et al. Secondary metabolites from Inula britannica L. and their biological activities. Molecule. 2010;15:1562–77.
[27] Zhao Y-M, Zhang M-L, Shi Q-W, Kiyota H. Chemical constituents of plants from the GenusInula. Chem Biodivers. 2006;3:371–84.
[28] Abdel-Hameed E-SS, Bazaid SA, Salman MS. Characterization of the phytochemical constituents of taif rose and its antioxidant and anticancer activities. BioMed Res Int. 2013;2013:1–13.
[29] Srinivasan R, Chandrasekar MJN, Nanjan MJ, Suresh B. Antioxidant activity of Caesalpinia digyna root. J Ethnopharmacol. 2007;113:284–91.
[30] Engwa GA. Free radicals and the role of plant phytochemicals as antioxidants against oxidative stress-related diseases. In: Asao T, Asaduzzaman M, editors. Phytochemicals – Source of Antioxidants and Role in Disease Prevention. United Kingdom: IntechOpen; 2018.
[31] Beauchamp C, Fridovich I. Superoxide dismutase: Improved assays and an assay applicable to acrylamide gels. Anal Biochem. 1971;44:276–87.
[32] Carrillo M-C, Kanai S, Nokubo M, Kitani K. (−) deprenyl induces activities of both superoxide dismutase and catalase but not of glutathione peroxidase in the striatum of young male rats. Life Sci. 1991;48:517–21.
[33] Paglia DE, Valentine WN. Studies on the quantitative and qualitative characterization of erythrocyte glutathione peroxidase. J Lab Clin Med. 1967;70:158–69.
[34] Alangari A, Alqahtani MS, Mateen A, Kalam MA, Alshememry A, Ali R, et al. Iron oxide nanoparticles: preparation, characterization, and assessment of antimicrobial and anticancer activity. Adsorp Sci Technol. 2022;2022:1–9.
[35] Aziz WJ, Abid MA, Hussein EH. Biosynthesis of CuO nanoparticles and synergistic antibacterial activity using mint leaf extract. Mater Technol. 2020;35:447–51.
[36] Priya DD. Aerva lanata-mediated bio-treated production of copper oxide nanoparticles, optimization by BBD–RSM method and it behaviour against water related mosquito. Appl Nanosci. 2021;11:207–16.
[37] Sharma JK, Akhtar MS, Ameen S, Srivastava P, Singh G. Green synthesis of CuO nanoparticles with leaf extract of Calotropis gigantea and its dye-sensitized solar cells applications. J Alloy Compd. 2015;632:321–5.
[38] Berne B, Pecora R. Dynamic light scattering with applications to chemistry. Biology, and Physics. Mineola, NY: Dover Publications; 2000.
[39] Pham-Huy LA, He H, Pham-Huy C. Free radicals, antioxidants in disease and health. Int J Biomed Sci. 2008;4:89–96.
[40] Sharifi-Rad M, Kumar ANV, Zucca P, Varoni EM, Dini L, Panzarini E, et al. Lifestyle, oxidative stress, and antioxidants: back and forth in the pathophysiology of chronic diseases. Front Physiol. 2020;11:694.
[41] Lobo V, Patil A, Phatak A, Chandra N. Free radicals, antioxidants and functional foods: Impact on human health. Phcog Rev. 2010;4:118.
[42] Young IS. Antioxidants in health and disease. J Clin Pathol. 2001;54:176–86.
[43] Morikawa T, Kitagawa N, Tanabe G, Ninomiya K, Okugawa S, Motai C. Quantitative determination of alkaloids in lotus flower (flower buds of nelumbo nucifera) and their melanogenesis inhibitory activity. Molecules. 2016;21:930.
[44] Paudel KR, Panth N. Phytochemical profile and biological activity of nelumbo nucifera. Evidence-Based Complement Alter Med. 2015;2015:1–16.
[45] Preethi DRA, Prabhu S, Ravikumar V, Philominal A. Anticancer activity of pure and silver doped copper oxide nanoparticles against A549 Cell line. Mater Today Commun. 2022;33:104462.
[46] Kalaiarasi A, Sankar R, Anusha C, Saravanan K, Aarthy K, Karthic S, et al. Copper oxide nanoparticles induce anticancer activity in A549 lung cancer cells by inhibition of histone deacetylase. Biotechnol Lett. 2018;40:249–56.
[47] Sella F, Sader E, Lolliot S, Cohen KR. Basic and advanced numerical performances relate to mathematical expertise but are fully mediated by visuospatial skills. J Exp Psychol: Learn Mem Cogn. 2016;42(9):1458.
[48] Eastman A, Barry MA. The origins of DNA breaks: A consequence of DNA Damage, DNA Repair, or Apoptosis?: New Drugs. Can Invest. 1992;10:229–40.
[49] Gökbulut A, Özhana O, Satılmiş B, Batçioğlu K, Günal S, Şarer E. Antioxidant and antimicrobial activities, and phenolic compounds of selected Inula species from Turkey. Nat Product Commun. 2013;8:1934578X1300800417.
[50] Herman A, Herman AP, Domagalska BW, Młynarczyk A. Essential oils and herbal extracts as antimicrobial agents in cosmetic emulsion. Indian J Microbiol. 2013;53:232–7.
[51] Khan RZSU AzamA, Farooqi IH. A study on effective adsorption of lead from an aqueous solution using Copper Oxide nanoparticles. IOP Conf Ser: Mater Sci Eng. 2021;1058:012074.
[52] Verma M, Tyagi I, Chandra R, Gupta VK. Adsorptive removal of Pb (II) ions from aqueous solution using CuO nanoparticles synthesized by sputtering method. J Mol Liq. 2017;225:936–44.
[53] Raul PK, Senapati S, Sahoo AK, Umlong IM, Devi RR, Thakur AJ, et al. CuO nanorods: a potential and efficient adsorbent in water purification. RSC Adv. 2014;4:40580–87.